ACADÉMIE
DES SCIENCES
INSTITUT DE FRANCE

Comptes Rendus
Physique

Manal Ahmed Awad, Khalid Mustafa Ortashi, Hayat Althobaiti and Nada Ali Almohawis

Green synthesis of Ag:ZnO nanoparticles via solvothermal method: characterization, photocatalytic and dielectric properties

Volume 27 (2026), p. 353-366

Online since: 28 August 2026

https://doi.org/10.5802/crphys.286

The Comptes Rendus. Physique *are a member of the Mersenne Center for open scientific publishing*
www.centre-mersenne.org — e-ISSN : 1878-1535

ACADÉMIE DES SCIENCES
INSTITUT DE FRANCE

Comptes Rendus. Physique
2026, Vol. 27, p. 353-366
https://doi.org/10.5802/crphys.286

Research article

Green synthesis of Ag:ZnO nanoparticles via solvothermal method: characterization, photocatalytic and dielectric properties

Manal Ahmed Awad [a,*], **Khalid Mustafa Ortashi** [b], **Hayat Althobaiti** [c] **and Nada Ali Almohawis** [d]

[a] King Abdullah Institute for Nanotechnology, King Saud University, Riyadh 11451, Saudi Arabia

[b] Department of Chemical Engineering, King Saud University, Riyadh, 11421, Saudi Arabia

[c] Department of Physics, College of Science, King Saud University, Riyadh 11451, Saudi Arabia

[d] Department of Chemistry, College of Science, King Saud University, P.O. 2455, Riyadh 11451, Saudi Arabia

E-mail: mawad@ksu.edu.sa (M. A. Awad)

Abstract. This study investigates the photocatalytic and dielectric properties of green-synthesized silver-doped zinc oxide nanoparticles (Ag:ZnONPs). FTIR analysis confirmed the presence of functional groups derived from the plant extract, which played a key role in the capping, and stabilization of the nanoparticles. SEM observations revealed rod-like and quasi-spherical nanostructures, while EDX analysis verified the successful incorporation of Ag into the ZnO matrix. XRD results confirmed the hexagonal wurtzite structure of synthesized sample, with an average crystallite size of approximately 20 nm. Photoluminescence studies showed near-band-edge emission with suppressed defect-related recombination, indicating improved charge carrier separation due to Ag doping. The Ag:ZnONPs demonstrated excellent visible-light photocatalytic performance, achieving nearly 99% degradation of crystal violet within 24 h and methyl orange within 72 h. Dielectric investigations revealed reduced impedance, and enhanced AC conductivity at room temperature, reflecting improved charge transport. The results highlight the multifunctional potential of green-synthesized Ag:ZnONPs for environmental remediation and advanced electronic applications.

Keywords. Ag:ZnONPs, Photocatalytic, Electrical properties.

Funding. Research Institute/Centre supporting program (ORF-RICSP-2026-1BT).

Manuscript received 21 January 2026, revised 13 May 2026 and 12 July 2026, accepted 28 July 2026, online since 28 August 2026.

1. Introduction

Nanomaterials have attracted significant scientific interest due to their unique physical and chemical properties that differ markedly from those of bulk materials. In particular, nanoparticles (NPs) exhibit high surface area, tunable band gaps, and enhanced catalytic activity, enabling

* Corresponding author

their application in gas sensing, photocatalysis, energy storage, electronics, antibacterial treatments, and environmental remediation [1]. As a result, increasing research efforts are focused on developing sustainable and eco-friendly nanomaterials, especially through green synthesis approaches, to overcome the limitations associated with conventional bulk materials and energy-intensive fabrication methods [2]. Among inorganic nanomaterials, zinc oxide (ZnO) nanoparticles have received considerable attention owing to their low cost, wide availability, and excellent physicochemical properties, including high surface area, optical transparency, wide band gap, and favorable electrochemical behavior. ZnO nanoparticles are widely used in photocatalysis, sensors, optoelectronic devices, pharmaceuticals, cosmetics, and ultraviolet light-emitting applications [3]. However, the synthesis route plays a critical role in determining the morphology, crystallinity, and functional performance of ZnO nanostructures. Conventional physical and chemical synthesis methods often involve high temperatures, toxic chemicals, hazardous solvents, and long reaction times, raising serious environmental and biological concerns. Green synthesis strategies using plant extracts have emerged as promising alternatives, offering environmentally benign, cost-effective, and biocompatible routes for nanoparticle fabrication. In plant-mediated synthesis, naturally occurring biomolecules act as reducing, capping, and stabilizing agents, minimizing toxicity while improving nanoparticle stability [4]. Various plant extracts have been successfully employed to synthesize metallic nanoparticles with applications in antibacterial, anticancer, antidiabetic, and tissue engineering fields [5]. The functional properties of ZnO nanoparticles can be further enhanced through elemental doping. In particular, silver (Ag) doping has been shown to improve optical, structural, antibacterial, and electrical properties by modifying defect states, reducing band gap energy, and enhancing charge transport [6]. Dielectric properties such as electric modulus, impedance, and AC conductivity are especially important for electronic and energy-storage applications [7]. This study is a continuation of our previous work [8]. In the present investigation, Trigonella extract was employed as a reducing and stabilizing agent for the green solvothermal synthesis of silver-doped zinc oxide nanoparticles (Ag:ZnONPs). The influence of key reaction parameters on nanoparticle formation was systematically examined. Comprehensive characterization using X-ray diffraction (XRD), UV–visible spectroscopy (UV–Vis), photoluminescence (PL) spectroscopy, Fourier transform infrared (FTIR) spectroscopy, scanning electron microscopy (SEM), and energy-dispersive X-ray spectroscopy (EDS) confirmed the successful synthesis, stabilization, and effective Ag incorporation. Furthermore, the photocatalytic activity and frequency-dependent electrical properties of the green-solvothermally synthesized Ag:ZnONPs were evaluated, demonstrating their strong potential for multifunctional applications.

2. Experimental

Ag-doped ZnO nanoparticles were synthesized using a green solvothermal approach following a previously reported method with slight modifications [8]. Trigonella seeds were washed, shade-dried, and ground into a fine powder, which was then extracted using a mixed ethanol–deionized water solvent system (11:5 v/v) under continuous stirring for 48 h. All reagents used were of analytical grade, and deionized water was employed throughout the synthesis. Three precursor solutions were prepared: 0.75 M NaOH, 1 mM $AgNO_3$ in ethanol, and 0.3 M zinc acetate dihydrate in ethanol. The zinc acetate solution was added to the Trigonella extract under stirring, followed by the gradual addition of $AgNO_3$ and NaOH until the pH reached 12. The reaction mixture was maintained at 80 °C for 2 h, leading to the formation of a brick-colored precipitate. The mixture was then transferred to a Teflon-lined autoclave and subjected to solvothermal treatment at 190 °C for 10 h. After cooling, the product was washed repeatedly with ethanol and deionized water, centrifuged, dried at 75 °C, and calcined at 400 °C to obtain Ag doped ZnO nanoparticles.

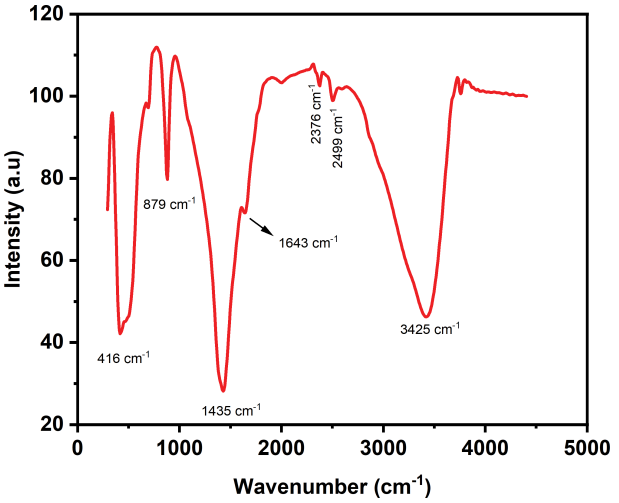

Figure 1. FTIR spectrum of Ag–ZnO nanoparticles [8].

The synthesized nanoparticles were comprehensively characterized to evaluate their structural, morphological, chemical, and electrical properties. Fourier Transform Infrared Spectroscopy (FTIR—Perkin-Elmer FTIR-spectrum BX, USA) was used to identify functional groups involved in nanoparticle stabilization, while scanning electron microscope (SEM, JEOL JSM-6360A instrument, Japan) analysis provided information on surface morphology and particle size distribution. Elemental composition was confirmed using energy dispersive spectroscopy (EDS, SEM, JEOL JSM-6400, Japan). Crystallographic structure and average crystallite size were determined by X-ray diffraction (XRD, D8 Advance X-ray diffractometer, Bruker, USA) analysis using Cu Kα radiation and the Scherrer equation. For dielectric studies, the Ag:ZnO nanopowder was fabricated into disc-shaped pellets using a PVA binder. Frequency-dependent electrical properties, including impedance, electric modulus, and AC conductivity, were measured at room temperature using a precision component analyzer, demonstrating the suitability of the synthesized Ag:ZnO nanoparticles for advanced functional applications.

3. Results and discussions

Figure 1 presents the FTIR spectrum of the green-synthesized Ag-doped ZnO nanoparticles recorded in the range of 400–4000 cm^{-1}, revealing the functional groups involved in nanoparticle formation and stabilization. A broad band at approximately 3425 cm^{-1} corresponds to O–H stretching vibrations, indicating the presence of surface hydroxyl groups and adsorbed water molecules. The absorption peak near 1643 cm^{-1} is attributed to N–H bending or C=C stretching vibrations of amine or aromatic groups originating from residual phytochemicals in the *Trigonella* extract [9]. Weak bands observed at 2376 and 2499 cm^{-1} are associated with organic residues, confirming the role of plant-derived biomolecules in the synthesis process. In the low wavenumber region, characteristic peaks between 645 and 416 cm^{-1} are assigned to Zn–O stretching vibrations, confirming the formation of the ZnO lattice [8]. Additional bands at around 1435 and 879 cm^{-1} correspond to C–H rocking and C–N stretching vibrations, respectively. The presence of carboxyl and methoxy groups highlights their role in the reduction, capping, and stabilization of Ag:ZnONPs during green synthesis [10].

Figure 2A shows the SEM micrograph of the green-synthesized Ag-doped ZnO nanoparticles, revealing a densely packed assembly of rod-like and quasi-spherical nanostructures with

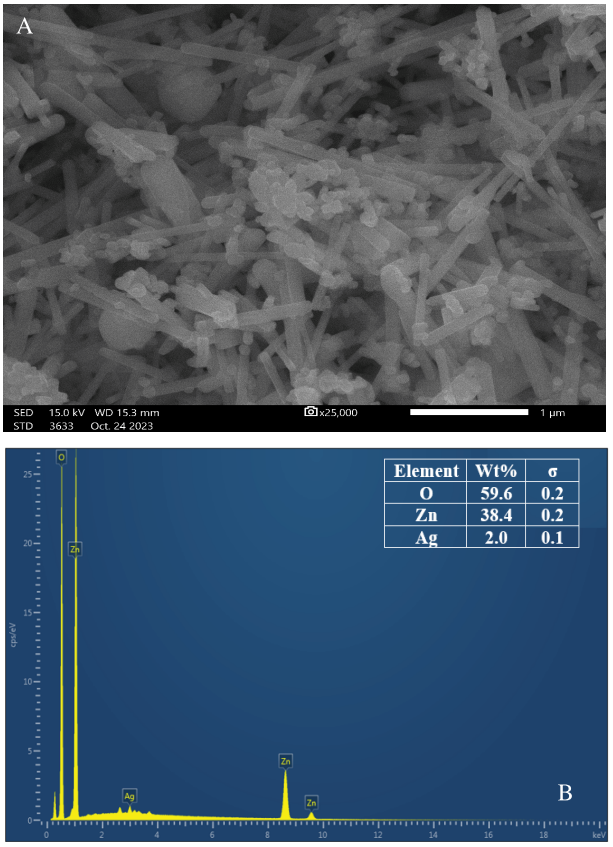

Figure 2. (A) SEM image, and (B) EDX analysis of Ag:ZnONPs [8].

nanoscale dimensions. The particles exhibit a relatively uniform distribution with noticeable agglomeration, which is commonly observed in metal-oxide nanoparticles synthesized via green routes due to surface energy effects and phytochemical capping [11]. Figure 2B presents the EDS spectrum of the Ag:ZnO nanoparticles, confirming the presence of Zn, O, and Ag as the principal elements, with no detectable impurity peaks. The characteristic Zn–K and O–K peaks confirm the presence of Zn and O elements associated with ZnO formation, whereas the appearance of Ag–L peaks indicates the presence of Ag in the synthesized sample [8]. The elemental composition obtained from EDS analysis, showing Zn and Oxygen as the dominant elements with a small but distinct silver (Ag) content, confirming effective Ag doping. The slight enrichment of Ag relative to theoretical values may be attributed to surface localization, highlighting the efficiency of the green synthesis approach [12].

Figure 3 illustrates the characteristic hexagonal wurtzite structure with P63mc symmetry of ZnO nanoparticles, exhibiting peaks at 2θ values of 31.64°, 34.45°, 36.23°, 47.61°, 56.62°, 62.97°, 66.45°, 67.85°, and 68.97°. These peaks correspond to the (100), (002), (101), (102), (110), (103), (200), (112), and (201) planes, respectively, and are in accordance with JCPDS, File No. 036-145145. Furthermore, two distinct peaks at 64.53° and 77.39° were found to correspond to the (202) and (004) planes of silver (Ag), respectively. The existence of Ag in the sample is confirmed by the fact that all the XRD peaks can be easily indexed to a face-centered cubic structure of Ag according to the literature (JCPDS, File No. 4-078346). Because the peak intensity of the Ag phase for Ag–ZnO nanoparticles became sharper and more intense as the Ag contents increased,

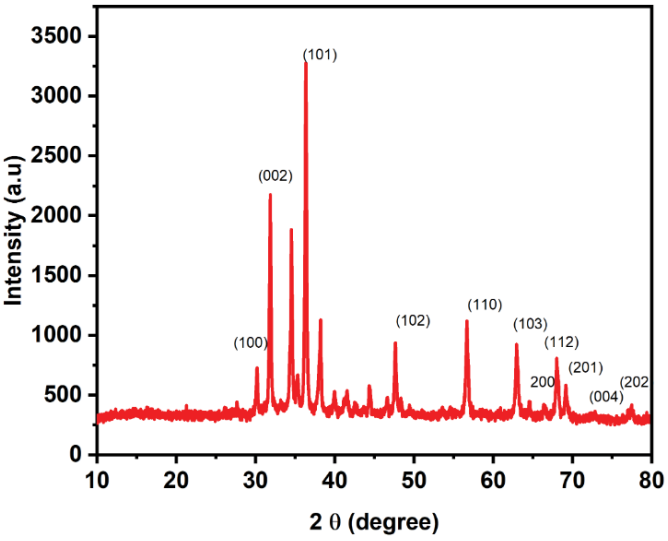

Figure 3. The XRD patterns of Ag:ZnONPs [8].

it may be inferred that the Ag metallic phase has been generated on the surface of the ZnO-NPs instead of being integrated into the ZnO complex. The crystallite size is 20 nm, calculated from the Scherrer formula. One possible explanation is that the synthesis of metallic Ag occurred due to the difference in ionic radius between Ag^{+} (126 pm) and Zn^{2+} (74 pm). Additionally, the fact that the peak locations of Ag–ZnO nanoparticles have not changed suggests that the Ag particles are located on the surfaces of the well-crystalline ZnO-NP [13].

The photoluminescence (PL) spectrum of the synthesized 1% Ag-doped ZnO nanoparticles was recorded in the wavelength range of 350–700 nm to investigate the optical emission behavior, defect structure, and charge-carrier recombination characteristics of the material. The PL spectrum exhibited three distinct emission peaks centered at approximately 397, 414, and 433 nm, along with a broad and weak visible emission band extending from approximately 470–600 nm (Figure 4). The emission peak observed at approximately 397 nm corresponds to the near-band-edge (NBE) ultraviolet emission of ZnO and is attributed to the radiative recombination of free excitons between the conduction and valence bands [14]. The intense emission peak centered at approximately 414 nm is associated with defect-related electronic transitions and may originate from shallow donor levels associated with zinc interstitials (Zn_i), oxygen antisite defects, or Ag-induced defect states within the ZnO lattice. The enhancement of this emission indicates that Ag doping modifies the electronic structure of ZnO by introducing localized energy states within the band gap. The relatively high intensity of this peak further suggests strong interaction between Ag dopants and the ZnO host lattice, as reported by [15]. The shoulder peak located at approximately 433 nm is attributed to blue emission associated with singly ionized oxygen vacancies (V_o^{+}), surface defects, or defect-assisted recombination processes. The presence of this peak further confirms the formation of intrinsic and extrinsic defect states resulting from Ag doping and nanoparticle synthesis. In addition, the broad weak visible emission band observed in the green region (approximately 470–600 nm) is commonly attributed to deep-level emissions originating from oxygen vacancies, lattice imperfections, and surface-related defects. These defect states play a significant role in influencing the photocatalytic, dielectric, and electrochemical properties of ZnO-based nanomaterials. The incorporation of Ag significantly affects the PL behavior of ZnO nanoparticles. Meng et al.; repotted that, Ag ions can act as electron-trapping

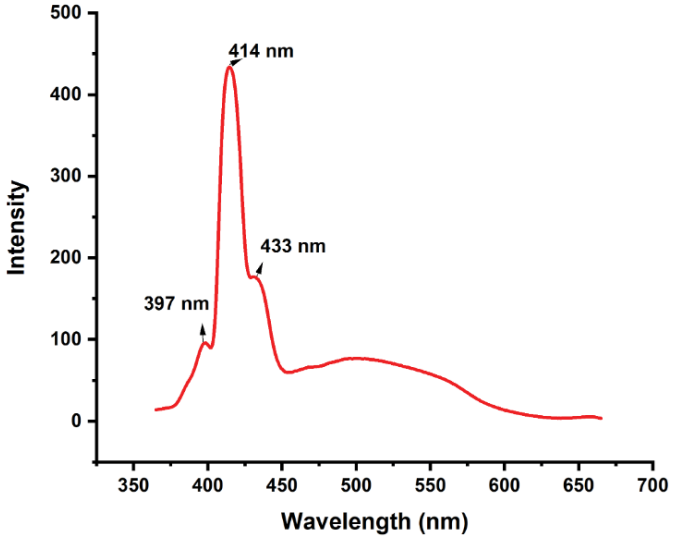

Figure 4. PL spectrum of synthesized Ag:ZnONPs.

centers, thereby suppressing the rapid recombination of photogenerated electron–hole pairs and promoting efficient charge separation [16]. This behavior is advantageous for photocatalytic and electrochemical applications, as it enhances charge-transfer efficiency and prolongs carrier lifetime.

The optical transmittance spectrum of the Ag-doped ZnO nanoparticles exhibits a pronounced absorption in the ultraviolet region followed by a sharp increase in transmittance at around 376 nm (see Figure 5), which corresponds to the fundamental absorption edge of ZnO. This absorption edge is associated with direct band-to-band electronic transitions. The low transmittance observed in the UV region is attributed to strong intrinsic ZnO absorption as well as the presence of defect-related states and Ag-induced electronic levels, which enhance light–matter interaction. Beyond the absorption edge, the transmittance gradually increases throughout the visible and near-infrared regions, reaching higher values at longer wavelengths due to the reduced photon energy being insufficient to promote electronic transitions. The moderate reduction in visible-light transmittance compared to pristine ZnO can be linked to Ag incorporation [17], which may introduce localized states and increase scattering at the nanoscale. Findings from [18] are in agreement with the effects of surface diffusion and agglomeration on the size and shape of Ag particles. According to reference [19], there is a surface plasmon resonance (SPR) absorption band in the 400–500 nm region in the optical transmission spectra of Ag:ZnO NPs. Reduced UV transmittance arises from intrinsic ZnO absorption and Ag-induced defects, while increased visible–NIR transmittance reflects modified optical response, enhancing photocatalytic and optoelectronic performance [20].

Ag-doped ZnO nanoparticles (Ag:ZnONPs) exhibited markedly enhanced visible-light photocatalytic activity compared with undoped ZnO. Nearly complete degradation (~99%) of crystal violet (CV) was achieved within 24 h, while the degradation of methyl orange reached ~99% within 72 h (Figure 6). The superior photocatalytic performance of Ag:ZnONPs is primarily attributed to Ag-induced surface plasmon resonance (SPR), which enhances visible-light absorption and facilitates efficient charge carrier separation [21]. Kinetic analysis further supports this enhancement, showing a higher apparent rate constant ($k \approx 6.2$ day^{-1}) and a shorter half-life ($t_{1/2} \approx 2.7$ h) for CV degradation. In contrast, methyl orange exhibited slower kinetics ($k \approx 2.3$ day^{-1}; $t_{1/2} \approx 7.2$ h),

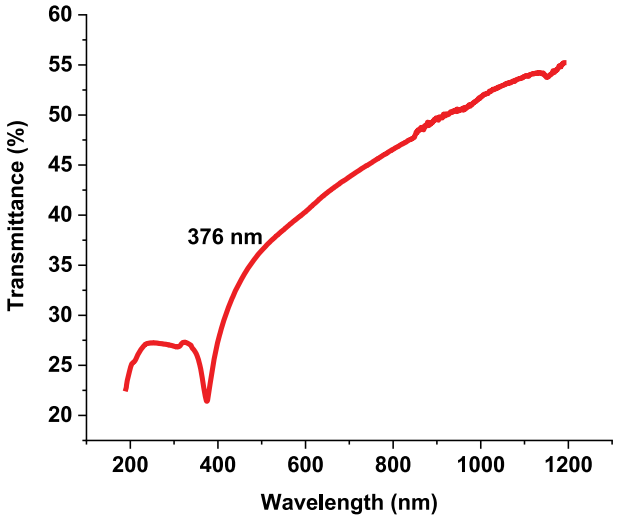

Figure 5. Transmittance spectrum of Ag:ZnONPs.

which can be attributed to the higher stability of its azo bonds; nevertheless, Ag doping significantly improved its degradation efficiency. The enhanced activity arises from the formation of a Schottky barrier at the Ag:ZnO interface, where Ag nanoparticles act as effective electron traps, suppressing electron–hole recombination. Upon light irradiation, photogenerated electrons are transferred from the ZnO conduction band to Ag, while holes remain in the valence band, promoting the generation of reactive oxygen species (ROS). Superoxide ($\bullet O_2^-$) and hydroxyl ($\bullet$OH) radicals, along with intermediate H_2O_2, actively attack and mineralize organic dye molecules into CO_2 and H_2O. These synergistic effects confirm that Ag incorporation significantly improves charge separation, ROS generation, and visible-light photocatalytic efficiency. The present results are in good agreement with earlier reports, demonstrating that Ag doping reduces recombination losses and SPR enhances visible-light-driven photocatalysis, making Ag:ZnONPs highly promising for environmental remediation applications [22–24].

The graph shows how the electric modulus changes as a function of frequency. The electric modulus spectra of green-synthesized Ag-doped ZnO nanoparticles reveal detailed information about bulk relaxation and charge transport mechanisms. In Figure 7A, the real part of the electric modulus (M') exhibits very low values at low frequencies ($M' \approx 0.00419$ at $\log f = 2$), indicating strong electrode polarization and high effective permittivity due to long-range mobility of charge carriers. With increasing frequency, M' gradually increases and reaches a maximum value of approximately 0.0376 at $\log f \approx 6.70$, signifying the suppression of electrode effects and the dominance of bulk (grain interior) response at higher frequencies. This monotonic increase in M' reflects a transition from long-range charge migration to localized hopping conduction [25]. The imaginary part of the electric modulus (M'') shows a clear relaxation behavior. At low frequencies, M'' remains small ($\approx$0.00374 at $\log f = 2$), then increases with frequency and reaches a maximum relaxation peak value of approximately $M''\max \approx 0.0160$ at $\log f \approx 6.70$. This peak corresponds to the characteristic relaxation frequency of the system and indicates conductivity-related relaxation associated with hopping of charge carriers and defect dipoles, particularly oxygen-vacancy-related centers introduced by Ag doping. The corresponding relaxation time, calculated using $\tau = 1/(2\pi f_{\max})$, is in the order of $\sim 10^{-7}$ s, confirming fast relaxation dynamics. The broad nature of the M'' peak suggests non-Debye relaxation behavior, indicating a distribution of relaxation times due to structural disorder, nanowire morphology, and heterogeneous

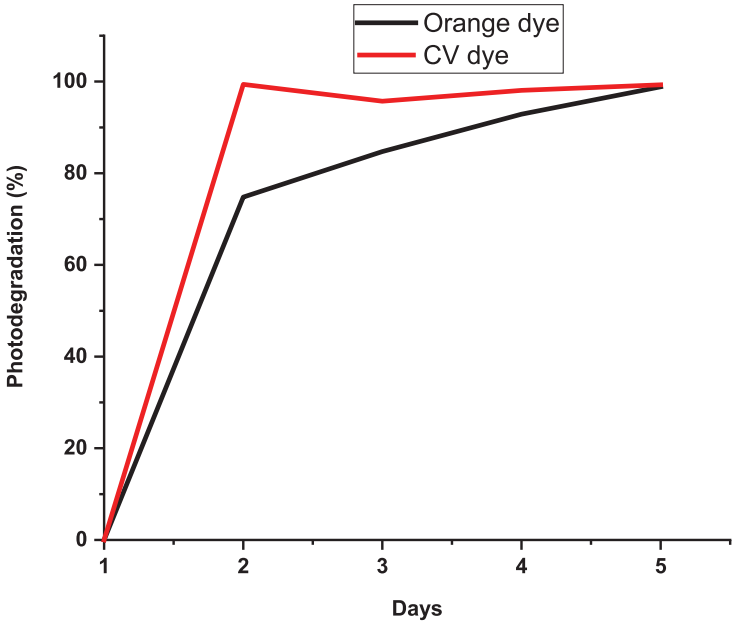

Figure 6. Photocatalytic performance of Ag:ZnONPs toward the degradation of CV and orange dyes.

conduction pathways. The combined M' and M'' behavior demonstrates that Ag incorporation enhances charge carrier density and defect-assisted transport, leading to improved electrical relaxation and bulk conductivity. These dielectric relaxation characteristics are highly favorable for electrochemical and energy storage applications, supporting the suitability of Ag–ZnO nanowires as advanced functional electrode materials [26,27].

The impedance behavior of the Ag:ZnONPs was analyzed using the frequency dependence of the real (Z') and imaginary (Z'') components of impedance (Figure 7B). At low frequencies (≈20–100 Hz), the real part of impedance (Z') exhibits a high value on the order of ~10^6–10^7 Ω, indicating significant resistance arising from grain boundaries, defect states, and space-charge polarization effects. As the frequency increases, Z' decreases sharply and reaches a much lower, nearly frequency-independent value of ~10^4 Ω in the high-frequency region (≈10^5–10^6 Hz). This pronounced reduction in Z' reflects enhanced charge carrier mobility and a decrease in grain boundary resistance, which can be attributed to the presence of Ag dopants that facilitate electron hopping and improve interfacial conductivity within the ZnO matrix.

Similarly, the imaginary part of impedance (Z'') shows a high magnitude at low frequencies, with values approaching ~10^6 Ω, and decreases continuously with increasing frequency, tending toward nearly zero at high frequencies. The absence of a distinct Z'' relaxation peak within the measured frequency range suggests a wide distribution of relaxation times and indicates non-Debye type relaxation behavior. The continuous suppression of Z'' with frequency implies reduced energy dissipation and faster polarization response of charge carriers under an alternating electric field. The simultaneous decrease in both Z' and Z'' with increasing frequency confirms that 1% Ag doping effectively lowers impedance, reduces resistive losses, and enhances charge transport in ZnO nanoparticles, making them promising candidates for applications in electronic devices, sensors, and photocatalytic systems where efficient charge transfer is required [28].

The AC conductivity (σ_{ac}) behavior of the 1% Ag-doped ZnO nanoparticles exhibits a strong dependence on frequency (see Figure 8), reflecting the underlying charge transport mechanisms

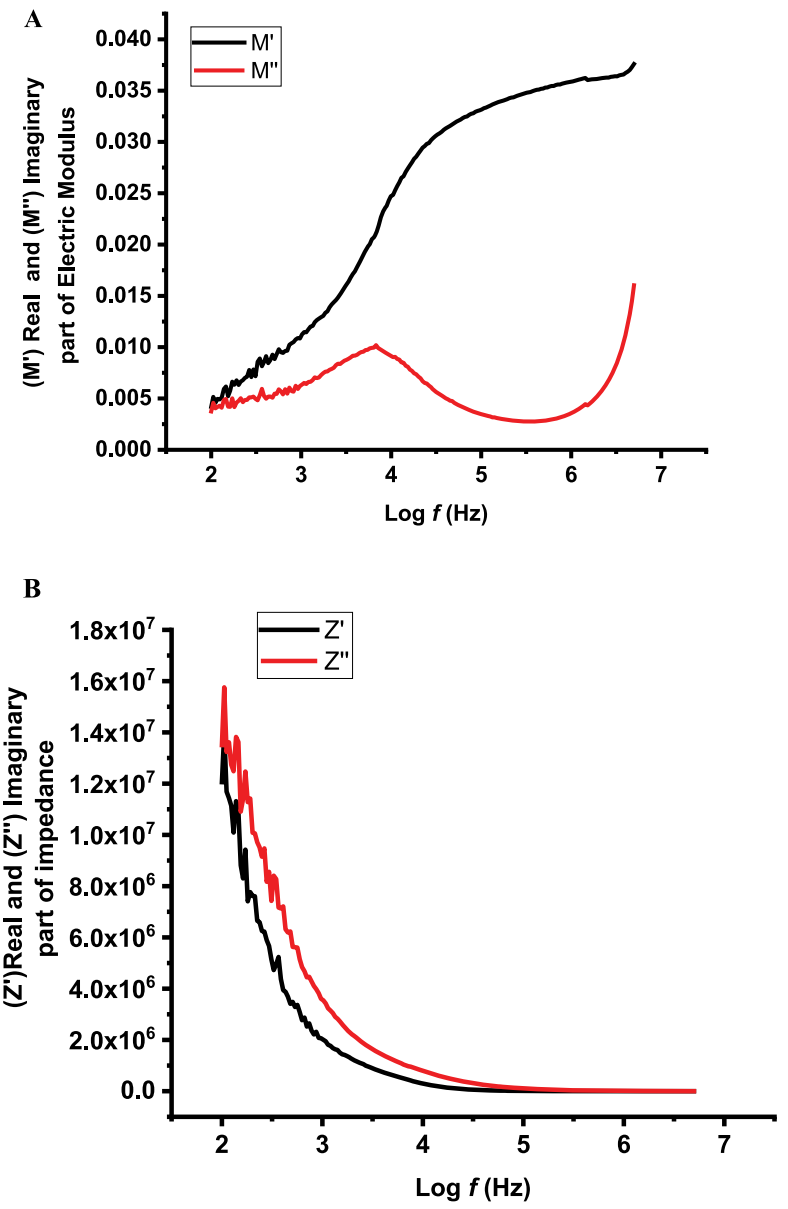

Figure 7. (A,B) Electric properties of Ag:ZnONPs.

in the material. At low frequencies (≈20–100 Hz), the AC conductivity shows relatively low values on the order of ~10^{-8}–10^{-7} S·cm^{-1}, which can be attributed to limited charge carrier mobility and the dominance of grain boundary resistance and space-charge polarization. As the frequency increases, σ_{ac} rises steadily and reaches values of approximately ~10^{-5}–10^{-4} S·cm^{-1} in the high-frequency region (≈10^5–10^6 Hz). This pronounced increase in conductivity with frequency indicates enhanced hopping of charge carriers between localized states and defect sites, consistent with a hopping conduction mechanism commonly observed in doped semiconducting oxides. The incorporation of Ag^+ ions into the ZnO lattice introduces additional localized energy levels and defect states, which facilitate charge carrier hopping and reduce potential barriers

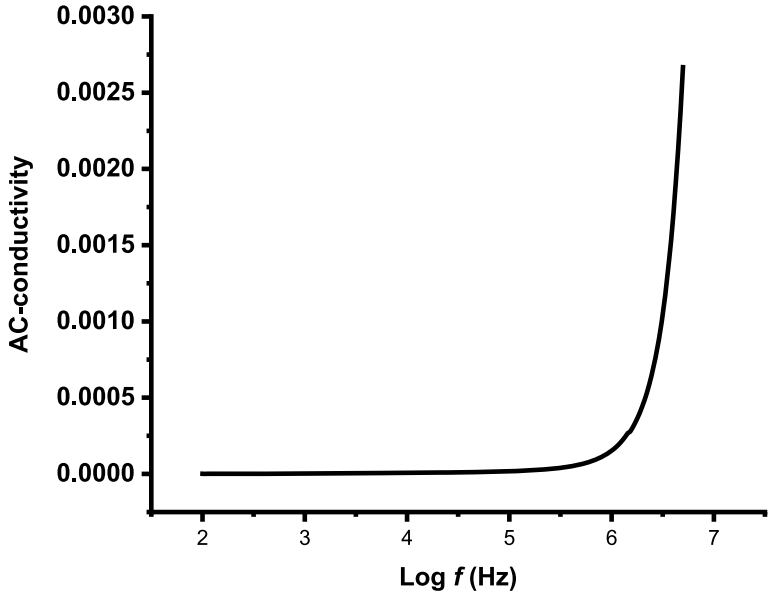

Figure 8. Variation of ac conductivity as a function of frequency for Ag:ZnONPs.

at grain boundaries [27]. Consequently, the improved AC conductivity at higher frequencies suggests more efficient charge transport and reduced resistive losses. The enhanced σ_{ac} values observed for the 1% Ag:ZnONPs confirm the beneficial role of Ag doping in improving electrical performance, making these materials promising for applications in electronic devices, sensors, and photocatalytic systems where frequency-dependent charge transport is critical [28].

The comparative Table 1 presents a literature-based overview of the physicochemical and functional properties of pure ZnONPs and Ag-doped ZnONPs synthesized using different preparation routes and doping concentrations. The comparison highlights the effect of Ag incorporation on the structural, optical, dielectric, electrical, and photocatalytic characteristics of ZnO nanomaterials. The reported studies indicate that Ag doping generally reduces the crystallite size and modifies the crystal structure through lattice distortion and defect formation. Optical investigations reveal changes in band gap energy and enhanced visible-light absorption due to Ag-induced localized surface plasmon resonance effects and defect-related energy states. PL analysis demonstrates that Ag incorporation suppresses electron–hole recombination by introducing defect levels and electron-trapping centers, leading to modified excitonic and defect-related emissions. Furthermore, Ag doping significantly improves electrical conductivity and dielectric properties by enhancing charge transport and interfacial polarization mechanisms. The photocatalytic performance of Ag-doped ZnONPs is also notably enhanced compared with pure ZnO due to improved charge separation efficiency and increased generation of reactive oxygen species [29,30].

4. Conclusions

In this study, green-synthesized silver-doped zinc oxide nanoparticles (Ag:ZnONPs) were successfully prepared and systematically investigated for their photocatalytic and dielectric properties. FTIR analysis confirmed the involvement of phytochemical functional groups from the Trigonella extract in the reduction, capping, and stabilization of the nanoparticles. SEM observations revealed rod-like and quasi-spherical nanostructures with nanoscale dimensions, while

Table 1. Comparative analysis of the structural, optical, PL, dielectric, and photocatalytic properties of pure ZnONPs and Ag-doped ZnONPs reported in previous studies

Pure ZnONPs					Ag doped ZnONPs						
Plasmonic signature (UV–vis) and band gap	Excitonic effects (PL)	Structural refinement average crystallite	Electrical properties	Photocatalytic performance	Doped %	Plasmonic signature (nm) and band gap (eV)	Excitonic effects (PL)	Structural refinement—average crystallite size (nm)	Electrical properties	Photocatalytic performance	Synthesis route
360 nm, 3.02 eV	Large exciton energy accelerates recombination	Hexagonal wurtzite—22.71 nm			10 wt%	450–55 nm, 2.90 eV	Ag traps electrons, reducing recombination	Hexagonal structure preserved; Ag growth confirmed—19.31 nm		98% methylene blue dye degradation under UV light in 60 min	*Carthamus tinctorius L.* leave [1]
372 nm, 3.19 eV		Hexagonal wurtzite—23 nm	Highest resistivity		5 wt%	361.5 nm, 3.27 eV		Wurtzite ZnO preserved with cubiic Ag—20 nm	Increase the conductivity		Aloe vera [2]
365 nm, 3.13 eV		Hexagonal wurtzite—23 nm	Supercapacitor performance		1%	374 nm, 2.88 eV		Improves crystallinity	Improves supercapacitor performance		Sansevieria trifasciata root [3]
374 nm, 3.72 eV	525 mm	Hexagonal wurtzite—16.5 nm	Lower conductivity than composit		≈50%	290 nm & 404 nm, 3.96 eV	Green emission band at 533 nm	Wuritzite ZnO preserved with cubic Ag—32.43 nm			*C. auriculata* leaf [4]

(continued on next page)

Table 1. (continued)

Pure ZnONPs					Ag doped ZnONPs						
Plasmonic signature (UV–vis) and band gap	Excitonic effects (PL)	Structural refinement average crystallite	Electrical properties	Photocatalytic performance	Doped %	Plasmonic signature (nm) and band gap (eV)	Excitonic effects (PL)	Structural refinement—average crystallite size (nm)	Electrical properties	Photocatalytic performance	Synthesis route
380 nm, 3.10 eV		Hexagonal wurtzite—28746	Resistance (Rp) = 104Ω	62% degradation of Tetracycline after 120 min	0.5%, 1%, 3%, 5%, and 7%	355.5 nm–360 nm (Ag at 416 nm)—Ag-0.5 %/ZnO (3.03 eV) > Ag-1%/ZnO (2.96 eV) > Ag-3%/ZnO (2.91 eV) > Ag-5%/ZnO (2.86 eV) > Ag-7%/ZnO (2.82 eV)		Ag accumulates at ZnO boundaries—22.768, 23.181, 26.052, 27.981, and 28.148; respectively	Resistance (Rp) = 46.9Ω	93% within the same 120-min	Morinda citrifolia fruit [5]
~375 nm, 3.24 eV	546 nm, 414 nm, 442, 464, and 490 nm	Hexagonal wurtzite, 25.945 nm	Moderate dielecteric constant, low conductivity		0.00, 0.02, 0.06, 0.12	Red-shifted, 3.21 eV, 3.17 eV, 3.18 eV; respectively	386 nm for 12 M% doping concentration	27.676, 32.174, 36.455 nm	Enhances (increases) both the dielectric constant and the AC conductivity		Chemical precipitation [6]
					1%		Defect-related emissions at 414 and 433 nm with suppressed electron–hole recombination due to Ag doping	Hexagonal wurtzite ZnO; rod-like and quasi-spherical nanoparticles; average crystallite size ≈20 nm	Reduced impedance, and enhanced AC conductivity at room temperature	≈99% degradation of crystal violet within 24 h and methyl orange within 72 h hunder visible-light irradiation	Green solvothermal method using Trigonella foenumgraecum seed extract [current sturdy]

EDX analysis verified the effective incorporation of Ag into the ZnO matrix without detectable impurities. XRD results confirmed the preservation of the hexagonal wurtzite structure of ZnO along with the presence of metallic Ag phases, and the average crystallite size was estimated to be ~20 nm. Photoluminescence studies demonstrated near-band-edge emission with suppressed defect-related recombination, indicating improved charge carrier separation due to Ag doping. The Ag:ZnONPs exhibited excellent visible-light photocatalytic performance, achieving nearly complete degradation of crystal violet and methyl orange dyes. Furthermore, dielectric investigations revealed non-Debye relaxation behavior, reduced impedance, and enhanced AC conductivity, reflecting improved charge transport characteristics. Overall, these findings demonstrate that green-synthesized Ag:ZnONPs are promising multifunctional materials for environmental remediation and advanced electronic applications.

Acknowledgements

The authors acknowledge the Research Institute/Centre supporting program (ORF-RICSP-2026-1BT), King Saud University, Riyadh, Saudi Arabia.

Declaration of interests

The authors do not work for, advise, own shares in, or receive funds from any organization that could benefit from this article, and have declared no affiliation other than their research organizations.

Data availability

All data are available upon request.

References

[1] Y. Khan, H. Sadia, S. Z. Ali Shah, et al., "Classification, synthetic, and characterization approaches to nanoparticles, and their applications in various fields of nanotechnology: a review", *Catalysts* **12** (2022), no. 11, article no. 1386.

[2] M. Zare, K. Namratha, S. Alghamdi, et al., "Novel green biomimetic approach for synthesis of ZnO–Ag nanocomposite; antimicrobial activity against food-borne pathogen, biocompatibility and solar photocatalysis", *Sci. Rep.* **9** (2019), no. 1, article no. 8303.

[3] A. A. Ansari, R. Lv, S. Gai, et al., "ZnO nanostructures – future frontiers in photocatalysis, solar cells, sensing, supercapacitor, fingerprint technologies, toxicity, and clinical diagnostics", *Coord. Chem. Rev.* **515** (2024), article no. 215942.

[4] S. Goswami, A. Bishnoi, D. Tank, et al., "Recent trends in the synthesis, characterization and commercial applications of zinc oxide nanoparticles—a review", *Inorg. Chim. Acta* **573** (2024), article no. 122350.

[5] H. R. El-Seedi, R. M. El-Shabasy, S. A. M. Khalifa, et al., "Metal nanoparticles fabricated by green chemistry using natural extracts: biosynthesis, mechanisms, and applications", *RSC Adv.* **9** (2019), article no. 24539.

[6] A. A. Shaikh, M. R. Patil, B. S. Jagdale and V. A. Adole, "Synthesis and characterization of Ag doped ZnO nanomaterial as an effective photocatalyst for photocatalytic degradation of Eriochrome Black T dye and antimicrobial agent", *Inorg. Chem. Commun.* **151** (2023), article no. 110570.

[7] F. Tayari, M. Benamara, M. Lal, et al., "Exploring enhanced structural and dielectric properties in Ag-doped Sr (NiNb) 0.5 O3 perovskite ceramic for advanced energy storage", *Ceramics* **7** (2024), no. 3, pp. 958–974.

[8] M. A. Awad, K. M. O. Ortashi, K. Alzahrani and H. Althobaiti, "Solvothermal eco-synthesis of Ag-Doped ZnO nanowires: investigation of structural, optical, dielectric, and electrochemical properties", *J. Taibah Univ. Sci.* **19** (2025), no. 1, pp. 1–13.

[9] M. Moond, S. Singh, S. Sangwan, P. Devi, A. Beniwal, J. Rani, A. Kumari and S. Rani, "Biosynthesis of silver nanoparticles utilizing leaf extract of Trigonella foenum-graecum L. for catalytic dyes degradation and colorimetric sensing of Fe^{3+}/Hg^{2+}", *Molecules* **28** (2023), no. 3, article no. 951.

[10] S. Pasieczna-Patkowska, M. Cichy and J. Flieger, "Application of Fourier transform infrared (FTIR) spectroscopy in characterization of green synthesized nanoparticles", *Molecules* **30** (2025), no. 3, article no. 684.

[11] T. Caguana, C. Cruzat, D. Herrera, D. Peña, V. Arévalo, M. Vera and E. Vanegas, "Metal nanoparticles obtained by green hydrothermal and solvothermal synthesis: characterization, biopolymer incorporation, and antifungal evaluation against Pseudocercospora fijiensis", *Nanomaterials* **15** (2025), no. 5, article no. 379.

[12] S. Dhiman, A. Kumari, R. Sharma, et al., "Green synthesis of Ag-doped ZnO nanoparticles using Bael (A. marmelos) leaves for wastewater remediation", *ECS J. Solid State Sci. Technol.* **13** (2024), no. 11, article no. 117001.

[13] S. S. R. Joya, S. N. Prerona, M. H. Kabir, A. Molla, M. F. Hossain and M. S. Rahman, "Eco-friendly synthesis of ZnO and Ag-doped ZnO nanoparticles using onion peel extract: characterization and comparative analysis", *ChemistrySelect* **10** (2025), no. 33, article no. e03084.

[14] S. J. Bailon-Ruiz, Y. Cedeño-Mattei, K. Torres-Torres and L. Alamo-Nole, "Photodegradation of tropaeolin O in the presence of Ag-doped ZnO nanoparticles", *Micro* **3** (2023), no. 3, pp. 643–652.

[15] A. Sedky, N. Afify, A. Almohammedi, E. M. M. Ibrahim and A. M. Ali, "Structural, optical, photoluminescence and magnetic investigation of doped and Co-doped ZnO nanoparticles", *Opt. Quant. Electron.* **55** (2023), no. 5, article no. 456.

[16] X. Meng, G. Fan, L. Xu, B. Zhang, Y. Chen, Y. Zhou, F. Xu and S. Zhang, "Ag-induced surface significant enhanced luminescence of ZnO thin films prepared by sol–gel coating", *Phys. B: Condens. Matter* **699** (2025), article no. 416864.

[17] D. Blažeka, R. Radičić, D. Maletić, S. Živković, M. Momčilović and N. Krstulović, "Enhancement of methylene blue photodegradation rate using laser synthesized Ag–ZnO nanoparticles", *Nanomaterials* **12** (2022), no. 15, article no. 2677.

[18] L. Xu, J. Miao, Y. Chen, J. Su, M. Yang, L. Zhang, L. Zhao and S. Ding, "Characterization of Ag–ZnO thin film for its potential applications in optoelectronic devices", *Optik* **170** (2018), pp. 484–491.

[19] A. Chelouche, D. Djouadi, H. Merzouk and A. Aksas, "Influence of Ag doping on structural and optical properties of ZnO thin films synthesized by the sol–gel technique", *Appl. Phys. A* **115** (2014), pp. 613–616.

[20] S. Kaenphakdee, S. Yodyingyong, J. Leelawattanachai, W. Triampo, N. Sanpo, J. Jitputti and D. Triampo, "Synthesis study of silver-doped zinc oxide for near-infrared shielding applications", in *Materials Science Forum*, vol. 1007, Trans Tech Publications Ltd.: Seoul, 2020, pp. 143–147.

[21] T. H. T. Vinh, N. T. B. Thuy, C. M. Thi and P. Van Viet, "Visible-light-driven photocatalysis of anisotropic silver nanoparticles decorated on ZnO nanorods: synthesis and characterizations", *J. Environ. Chem. Eng.* **9** (2021), no. 2, article no. 105103.

[22] A. W. Digisu, A. Berhe Yaebyo, W. L. Kebede, H. M. Ahmed and T. Fentie Yemir, "Photocatalytic performance of silver-doped zinc oxide nanoparticles for methylene blue degradation", *Catal. Lett.* **155** (2025), no. 3, article no. 100.

[23] P. Midya, P. P. Sarngan, A. Dutta, K. K. Chattopadhyay and D. Sarkar, "Carbon-modified TiO_2 nanourchin with Ag nanoparticle decoration for environmental remediation", *Mater. Sci. Eng. B* **286** (2022), article no. 116028.

[24] S. Ezendam, M. Herran, L. Nan, et al., "Hybrid plasmonic nanomaterials for hydrogen generation and carbon dioxide reduction", *ACS Energy Lett.* **7** (2022), no. 2, pp. 778–815.

[25] S. Sagadevan, K. Pal, Z. Z. Chowdhury and M. E. Hoque, "Structural, dielectric and optical investigation of chemically synthesized Ag-doped ZnO nanoparticles composites", *J. Sol–Gel Sci. Technol.* **83** (2017), no. 2, pp. 394–404.

[26] M. Khatun and E. Kabir, "Dielectric relaxation and electrical conductivity in lead-free organic ferroelectric diisopropylammonium bromide (dipaBr)", *Solid State Commun.* **393** (2024), article no. 115670.

[27] T. Frömling, Y. Liu, A. P. Hoang, M. Gehringer, S. Steiner, M. Zhuk, J. Glaum and B. X. Xu, "Modulus spectroscopy for the detection of parallel electric responses in electroceramics", *J. Materiomics* **8** (2022), no. 3, pp. 556–569.

[28] Y. Zhang, W. Li, S. Zhang, X. Tang, Q. Liu, Y. Jiang, Z. Tang and X. Guo, "The dielectric relaxation and impedance spectroscopy analysis of (Bi0. 5Na0. 5 TiO_3-based ceramics", *Mater. Res. Bull.* **153** (2022), article no. 111874.

[29] J. J. Ma, Y. Gao, Y. Chen and M. H. Wang, "Effects of (Ag, Ta) doping on the microstructure and dielectric properties of titanium dioxide functional ceramics", *J. Electron. Mater.* **52** (2023), no. 6, pp. 3698–3705.

[30] G. Khamidov and İ. Erol, "Incorporation of Ag and ZnO nanoparticles produced by green synthesis into carboxymethyl cellulose-based polymer blend: investigation of dielectric and surface properties", *Funct. Compos. Struct.* **7** (2025), no. 3, article no. 035008.